Airborne Observations Constrain Heterogeneous Nitrogen and Halogen Chemistry on Tropospheric and Stratospheric Biomass Burning Aerosol

Zachary C. J. Decker[1,2,3,4], Gordon A. Novak[1,2], Kenneth Aikin[1,2], Patrick R. Veres[1,5], J. Andrew Neuman[1,2], Ilann Bourgeois[1,2,6], T. Paul Bui[7], Pedro Campuzano-Jost[2,3], Matthew M. Coggon[1,2], Douglas A. Day[2,3], Joshua P. DiGangi[8], Glenn S. Diskin[8], Maximilian Dollner[9], Alessandro Franchin[1,2,10], Carley D. Fredrickson[11], Karl D. Froyd[1,2], Georgios I. Gkatzelis[1,2,12], Hongyu Guo[2,3], Samuel R. Hall[10], Hannah Halliday[8], Katherine Hayden[13], Christopher D. Holmes[14], Jose L. Jimenez[2,3], Agnieszka Kupc[1,2,9], Jakob Lindaas[15], Ann M. Middlebrook[1], Richard H. Moore[8], Benjamin A. Nault[16], John B. Nowak[8], Demetrios Pagonis[2,3,17], Brett B. Palm[5,11], Jeff Peischl[1,2], Felix M. Piel[18,19], Pamela S. Rickly[1,2,20], Michael A. Robinson[1,2,3], Andrew W. Rollins[1], Thomas B. Ryerson[1], Gregory P. Schill[1], Kanako Sekimoto[21], Chelsea R. Thompson[1], Kenneth L. Thornhill[8,22], Joel A. Thornton[11], Kirk Ullmann[10], Carsten Warneke[1], Rebecca A. Washenfelder[1,23], Bernadett Weinzierl[9], Elizabeth B. Wiggins[8], Christina J. Williamson[1,2,24,25], Edward L. Winstead[8,22], Armin Wisthaler[18,19], Caroline C. Womack[1,2], and Steven S. Brown[1,3]

[1]NOAA Chemical Sciences Laboratory (CSL), Boulder, CO, USA, [2]Cooperative Institute for Research in Environmental Sciences, University of Colorado Boulder, Boulder, CO, USA, [3]Department of Chemistry, University of Colorado Boulder, Boulder, CO, USA, [4]Now at Laboratory of Atmospheric Chemistry, Paul Scherrer Institute (PSI), Villigen, Switzerland, [5]Now at National Center for Atmospheric Research, Boulder, CO, USA, [6]Now at Université Savoie Mont Blanc, INRAE, CARRTEL, Thonon-les-Bains, France, [7]NASA Ames Research Center, Moffett Field, CA, USA, [8]NASA Langley Research Center, Hampton, VA, USA, [9]Faculty of Physics, Aerosol Physics and Environmental Physics, University of Vienna, Vienna, Austria, [10]Atmospheric Chemistry Observations and Modeling Laboratory, National Center for Atmospheric Research, Boulder, CO, USA, [11]Department of Atmospheric Sciences, University of Washington, Seattle, WA, USA, [12]Now at Institute of Energy and Climate Research, IEK-8: Troposphere, Forschungszentrum Jülich GmbH, Jülich, Germany, [13]Air Quality Research Division (AQRD), Environment and Climate Change Canada, Toronto, ON, Canada, [14]Department of Earth, Ocean, and Atmospheric Science, Florida State University, Tallahassee, FL, USA, [15]Department of Atmospheric Science, Colorado State University, Fort Collins, CO, USA, [16]Center for Aerosol and Cloud Chemistry, Aerodyne Research, Inc., Billerica, MA, USA, [17]Now at Department of Chemistry and Biochemistry, Weber State University, Ogden, UT, USA, [18]Institute for Ion Physics and Applied Physics, University of Innsbruck, Innsbruck, Austria, [19]Department of Chemistry, University of Oslo, Oslo, Norway, [20]Now at Colorado Department of Public Health and Environment, Denver, CO, USA, [21]Graduate School of Nanobioscience, Yokohama City University, Yokohama, Japan, [22]Science Systems and Applications, Inc. (SSAI), Hampton, VA, USA, [23]Now at Cooperative Institute for Research in Environmental Sciences, University of Colorado Boulder, Boulder, CO, USA, [24]Now at Finnish Meteorological Institute, Helsinki, Finland, [25]Now at Institute for Atmospheric and Earth System Research/Physics, Faculty of Science, University of Helsinki, Helsinki, Finland

Abstract Heterogeneous chemical cycles of pyrogenic nitrogen and halides influence tropospheric ozone and affect the stratosphere during extreme Pyrocumulonimbus (PyroCB) events. We report field-derived N_2O_5 uptake coefficients, $\gamma(N_2O_5)$, and $ClNO_2$ yields, $\varphi(ClNO_2)$, from two aircraft campaigns observing fresh smoke in the lower and mid troposphere and processed/aged smoke in the upper troposphere and lower stratosphere (UTLS). Derived $\varphi(ClNO_2)$ varied across the full 0–1 range but was typically <0.5 and smallest in a PyroCB (<0.05). Derived $\gamma(N_2O_5)$ was low in agricultural smoke (0.2–3.6×10^{-3}), extremely low in mid-tropospheric wildfire smoke (0.1×10^{-3}), but larger in PyroCB processed smoke (0.7–5.0×10^{-3}). Aged biomass burning aerosol in the UTLS had a higher $\gamma(N_2O_5)$ of 17×10^{-3} that increased with sulfate and liquid water, but that was 1–2 orders of magnitude lower than values for aqueous sulfuric aerosol used in stratospheric models.

Plain Language Summary The injection of reactive material into Earth's atmosphere from fires affects atmospheric composition at regional and hemispheric scales. Reported stratospheric ozone depletion during extreme events, such as the 2020 Australian wildfires, illustrates one example of fire impacts and the role of heterogeneous (gas-particle) processes. We report field quantification of rates and product yields from

airborne observations of smoke. Extremely slow heterogeneous reaction rates on young smoke increase with transport and aging, but upper atmospheric values are still a factor of 10 slower than parameterizations used in stratospheric models. Heterogeneous production of $ClNO_2$, a major lower atmospheric chlorine activation pathway, may be active on biomass burning aerosol in the upper atmosphere.

1. Introduction

Biomass burning (BB) impacts global atmospheric chemical processes and is increasing regionally due to climate-change-induced trends in fire weather (Jones et al., 2022). Fires emit nitrogen oxides ($NO + NO_2 = NO_x$), volatile organic compounds (VOCs) and aerosol that affect tropospheric oxidants (Koss et al., 2018). Roughly 10% of global inorganic chloride enters the atmosphere by BB (Wang et al., 2019), and a small fraction of this may be subsequently activated to inorganic chlorine radicals. The co-emission of NO_x and VOCs enhances tropospheric O_3 globally on a scale comparable to, or greater than, urban pollution (Bourgeois et al., 2021; Xu et al., 2021).

Large wildfires can form smoke-filled thunderstorm clouds called pyrocumulonimbus (PyroCB) towers (Peterson et al., 2021, 2022) that loft pyrogenic emissions to the upper troposphere/lower stratosphere (UTLS). Aerosol injection from the 2019–2020 Australian New Year fires altered the partitioning of total reactive chlorine (Cl_y) and nitrogen (NO_y) species and led to stratospheric O_3 loss (Bernath et al., 2022; Solomon et al., 2022, 2023; Strahan et al., 2022). This O_3 depletion results from heterogeneous reactions on the particulate surface area of injected BB material. One of the major heterogeneous reactions is the uptake of N_2O_5, which in stratospheric models produces exclusively nitric acid, HNO_3 (Küll et al., 2002; Zambri et al., 2019).

$$N_2O_{5(g)} + H_2O_{(l)} \rightarrow 2HNO_{3(g)} \qquad (R1, \gamma)$$

The uptake coefficient, γ, is the probability for reactive uptake upon a gas-particle collision (Ravishankara, 1997). Production of N_2O_5 occurs primarily in the absence of sunlight due to the photochemical instability of its nitrate radical (NO_3) precursor (Brown & Stutz, 2012). Reaction 1 influences NO_x and O_3 in both the stratosphere and troposphere by altering the partitioning of reactive nitrogen and the availability of NO_x (Dentener & Crutzen, 1993; Solomon, 1999).

Tropospheric observations have shown substantial yields of nitryl chloride, $ClNO_2$, from chloride-containing aerosol (McDuffie et al., 2018b), represented below as reaction with HCl.

$$N_2O_{5(g)} + HCl_{(aq)} \rightarrow ClNO_{2(g)} + HNO_{3(g)} \qquad (R2, \phi)$$
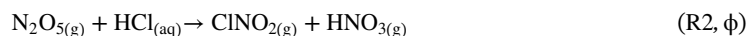
Subsequent photolysis of $ClNO_2$ produces Cl. The yield, ϕ, for R2 is the molar ratio of $ClNO_2$ produced per N_2O_5 reacted. Due in part to the lack of chloride partitioning to highly-acidic stratospheric aerosol, R2 has been considered an unimportant contribution to stratospheric halogen activation (Solomon, 1999) despite its prevalence in the troposphere. Figure 1 illustrates BB emissions to different regions of the atmosphere together with the emissions and heterogeneous chemistry described above with results described below.

There is considerable uncertainty caused by a lack of experimentally-derived rates and yields related to N_2O_5 heterogeneous chemistry on BB particles (Solomon et al., 2022; Strahan et al., 2022; Yu et al., 2021). Current models assume BB particles are similar to volcanic particles but are unable to reproduce the remote sensing observations of Cl_y and NO_y, suggesting substantial differences in N_2O_5 heterogeneous chemistry. Values of γ (N_2O_5) and $\varphi(ClNO_2)$ for BB aerosol are poorly constrained. To our knowledge there no field-derived values. There exist limited BB laboratory studies on $\gamma(N_2O_5)$ or $\varphi(ClNO_2)$, which suggest $\gamma(N_2O_5)$ and $\varphi(ClNO_2)$ can be altered by aerosol organic content and inorganic salts (e.g., nitrate and chloride) (Ahern et al., 2018; Goldberger et al., 2019; Jahl et al., 2021). Current tropospheric and stratospheric models used to study BB impacts are poorly constrained for $\gamma(N_2O_5)$ and have not considered $ClNO_2$ formation.

Here, we present aircraft observations of $ClNO_2$ and N_2O_5 and field-derived values for $\gamma(N_2O_5)$ and $\varphi(ClNO_2)$ in BB smoke. The analysis combines model and parameterization methods with aircraft observations from two field campaigns: the 2019 Fire Influence on Regional to Global Environments and Air Quality (FIREX-AQ) campaign
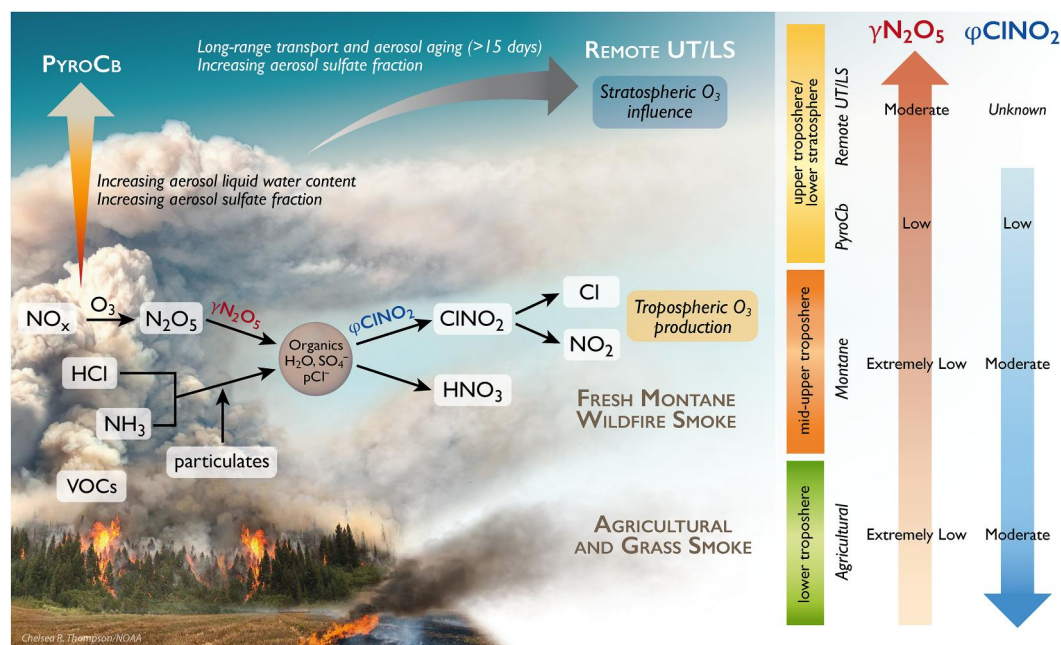
Figure 1. Illustration of biomass burning sources and emission to different regions of the atmosphere together with the heterogeneous chemistry of N_2O_5 and $ClNO_2$. Arrows on the right-hand side illustrate trends in heterogeneous parameters, γ (N_2O_5) and $\phi(ClNO_2)$, determined from aircraft observations in this work.

(Warneke et al., 2023) and the 2017–2018 Atmospheric Tomography Mission (ATom) (Thompson et al., 2022). We derive $\gamma(N_2O_5)$ and $\varphi(ClNO_2)$ for fresh montane- and agricultural-fueled smoke emissions in the troposphere and a PyroCB injection of smoke to the upper troposphere from observations of daytime N_2O_5 and $ClNO_2$ during FIREX-AQ. We derive $\gamma(N_2O_5)$ for stratospheric BB-influenced aerosol from ATom. Derived N_2O_5 uptake coefficients are considerably lower than current model parameterizations. Halogen activation through $ClNO_2$ from NO_x and particulate chloride (pCl^-) is prevalent in low altitudes and possible, yet unquantified, at high altitude. We discuss the factors that govern this heterogeneous chemistry in young and aged smoke.

2. Data and Methods

2.1. Observations

FIREX-AQ was a large-scale field research campaign focusing on wildfire smoke plumes in the western U.S. and prescribed agricultural burning smoke plumes in the southeastern U.S. during the summer of 2019. We use observations from the NOAA Chemistry Twin Otter and NASA DC-8 aircraft (see Text S1.1 in Supporting Information S1). The NASA Atmospheric Tomography (ATom) mission was a large-scale research campaign focusing on remote tropospheric, UTLS, and stratospheric air (Thompson et al., 2022). Data here are from September–October 2017 (ATom-3) and April–May 2018 (ATom-4) (Text S1.2 in Supporting Information S1). Table S1 in Supporting Information S1 lists instrumentation used in this analysis. In situ observations from ATom and FIREX-AQ are available as a merged data set and found in Wofsy et al. (2018) and Warneke et al. (2023), respectively. See further details in Supporting Information S1.

2.2. Models and Parameterizations

Two models are used: an iterative 0-D box model constrained to crosswind transects of wildfire plumes sampled during FIREX-AQ (Decker, Robinson, et al., 2021) (Text S1.3 in Supporting Information S1) and an iterative diel model constrained to observations for each parcel of sampled air (McDuffie et al., 2018b) above an arbitrary elevation cutoff of 6 km during ATom-3 and ATom-4 (Text S1.3 in Supporting Information S1). Calculated φ ($ClNO_2$) uses a parameterization determined from laboratory experiments (Bertram et al., 2009; Roberts et al., 2009) (Text S1.4 in Supporting Information S1). See further details in the SI.
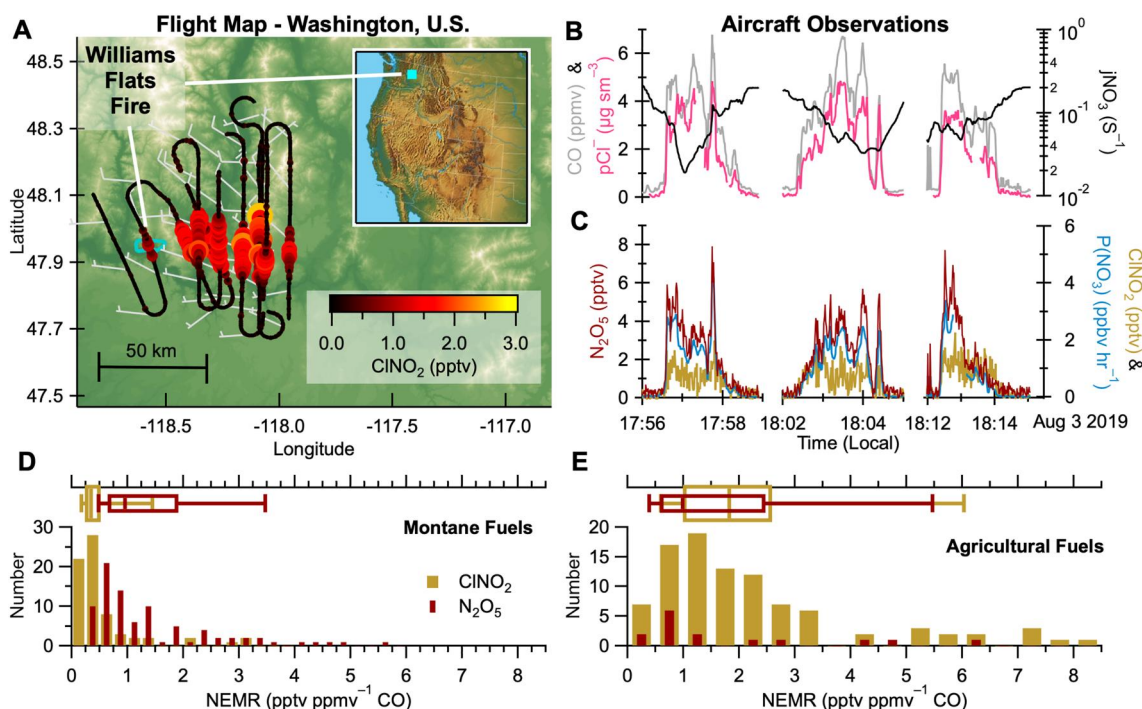
Figure 2. (a) NASA DC-8 flight tracks colored and sized by $ClNO_2$ mixing ratio for the Williams Flats fire plume on Aug 3. The inset map shows the approximate location of sampling in Washington State. (b) Observations of CO (gray), pCl^- (pink), and jNO_3 (black) and (c) N_2O_5 (red), $ClNO_2$ (yellow) and $P(NO_3)$ (blue) for a subset of crosswind plume transects. (d and e) Histogram of N_2O_5 and $ClNO_2$ NEMRs from all montane (d) and agricultural (e) fires. Box plots show 10th, 25th, 50th, 75th, and 90th percentiles.

3. Results and Discussion

3.1. $ClNO_2$ and N_2O_5 Observations

During FIREX-AQ the NOAA I^- CIMS aboard the DC-8 measured mixing ratios of N_2O_5 and $ClNO_2$ up to 19 and 3 parts per trillion by volume (pptv), respectively, in near-field (<5 hr transport time) daytime plumes. Figure 2a shows the flight track of the NASA DC-8 aircraft sampling the Williams Flats fire on 3 August colored and sized by observed $ClNO_2$. Both N_2O_5 and $ClNO_2$ exhibit clear enhancements despite significant photolysis rates of NO_3 (jNO_3) (Figures 2b and 2c). These enhancements are associated with CO, a smoke tracer, and rapid (>1 ppbv hr^{-1}) NO_3 production, $P(NO_3) = k[NO_2][O_3]$, where k is the bimolecular rate coefficient for reaction of NO_2 with O_3.

Median j_{NO_3} at the center of wildfire and agriculture plume transects (0.14 and 0.19 s^{-1} respectively) presented here were 15%–30% lower than values outside of plumes (0.16 and 0.20 s^{-1} respectively). In large wildfire plumes jNO_3 attenuation was a factor of 10 or more (Figures 2b and 2c), but small agricultural plumes exhibited no attenuation (Figure S1 in Supporting Information S1). Previous analyses of FIREX-AQ plumes found that NO_3 photolysis and reaction with NO are not major NO_3 loss pathways regardless of time of day (Decker, Robinson, et al., 2021) and that NO_3 chemistry is active regardless of the location at plume center or edge (Decker, Wang, et al., 2021). Rapid $P(NO_3)$ together with large concentrations of highly reactive VOCs and aerosol surface area control NO_3 and N_2O_5 chemistry. Plumes with measurable daytime N_2O_5 provide measures of NO_3 reactivity and N_2O_5 heterogeneous uptake for these species that are otherwise important only at night in non-fire environments.

The Normalized Excess Mixing Ratio (NEMR, see Text S1.5 in Supporting Information S1) measures the above background enhancements of a compound x relative to the smoke tracer CO (Table S2 and Figures S2–S4 in Supporting Information S1). The median N_2O_5 NEMR was 1.0 pptv $ppmv^{-1}$ CO for both agricultural- and montane-fueled fire groups (Figures 2d and 2e). The $ClNO_2$ NEMRs, by contrast, differ by a factor of ~6 between montane (0.3 pptv $ppmv^{-1}$) and agricultural (1.8 pptv $ppmv^{-1}$) fuels. Agricultural and grass burning emits more Cl^- per kg of fuel burned (emission factor) when compared to temperate and boreal forest burning (Akagi
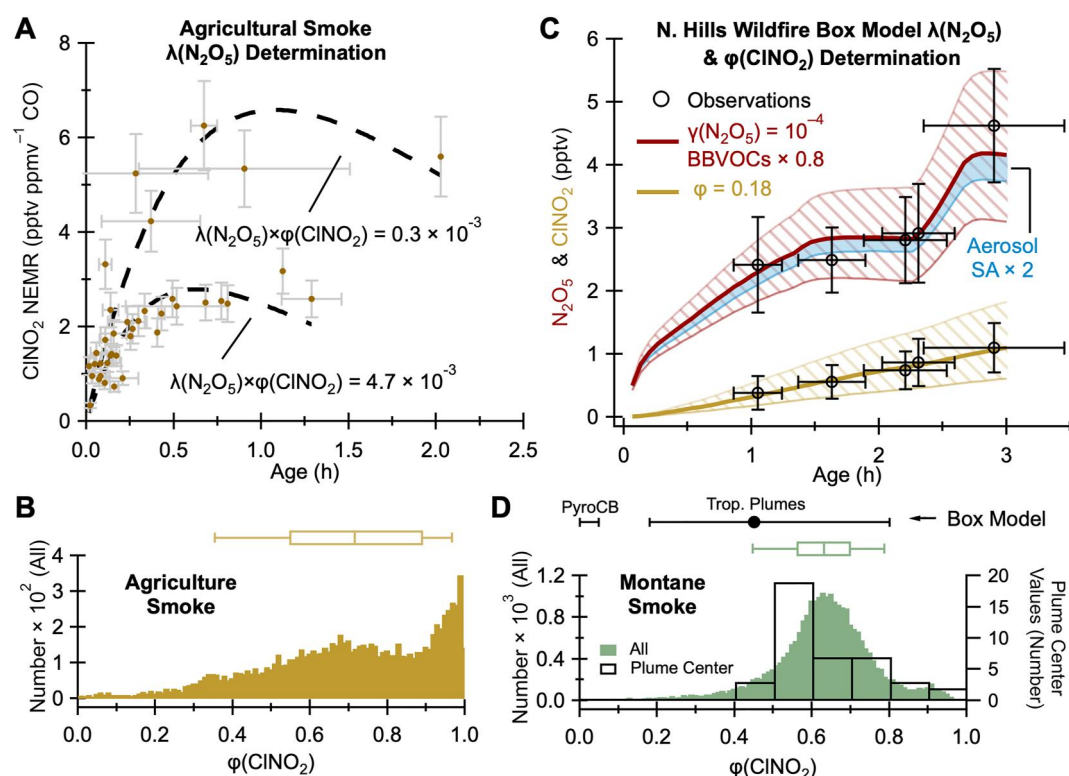
Figure 3. (a) Calculated ClNO$_2$ NEMRs from agricultural-fueled fires versus plume age. Each marker is the Normalized Excess Mixing Ratio of a single plume transect. Dashed lines show biexponential fits (see text). (b) Parametrized φ(ClNO$_2$) of agricultural smoke. (c) Box model results (lines) compared to observations (markers) of N$_2$O$_5$ and ClNO$_2$ from the July 29 North Hills smoke plume with γ(N$_2$O$_5$) = 10^{-4}. The hashed area shows changes to volatile organic compounds (N$_2$O$_5$) or yield (ClNO$_2$) that encompass observational uncertainty. Sensitivity to an aerosol surface area factor of 2 increase, considered the maximum increase in surface area from water corrections, is shown by a transparent blue area. The apparent discontinuity of N$_2$O$_5$ in the model is due to a reduction in the photolysis rate at sunset (2.5 hr of age). (d) Parameterized φ (ClNO$_2$) for montane smoke (filled bars) and transect center observations used in the box model (empty bars). Box model derived φ(ClNO$_2$) is shown as horizontal ranges in black. The black marker indicates the average of the five modeled plumes sampled in the lower troposphere. The range on the model-derived φ(ClNO$_2$) shows the range of the five modeled plumes. Note that within observation uncertainty the full range is 0–1.

et al., 2011; Liu et al., 2016; May et al., 2014). Despite considerable variability, the greater median λClNO$_2$ NEMR for agricultural-fueled fires is consistent with the observed differences in particulate chloride (pCl$^-$). DC-8 and Twin Otter observations of the above background pCl$^-$ show that agricultural and grass smoke contains roughly 16× more pCl$^-$ by mass than montane smoke (Text S2 and Figure S5 in Supporting Information S1). The majority of pCl$^-$ is from KCl emissions, which is quantitatively detectable in the AMS.

3.2. Montane and Agricultural Smoke

To derive γ(N$_2$O$_5$) from agricultural smoke, we use the calculated NEMR of ClNO$_2$ as a function of the physical plume age (Text S1.1 in Supporting Information S1) shown in Figure 3a. We combine the calculated ClNO$_2$ NEMRs with the relationship between γ(N$_2$O$_5$) and φ(ClNO$_2$) below to estimate a γ(N$_2$O$_5$).

$$\gamma(\mathrm{N_2O_5}) = 4 \times \frac{k_{\mathrm{N_2O_5}}}{c \times \mathrm{SA}} \tag{1}$$

$$\phi(\mathrm{ClNO_2}) = \frac{k_{\mathrm{ClNO_2}}}{k_{\mathrm{N_2O_5}}} \tag{2}$$

Here c is the mean molecular speed of N$_2$O$_5$ and SA is the aerosol surface area density. Data are separated into low and high NEMR groups, although we are unable to identify any metric that differentiates the two groups. The

biexponential fit represents first-order formation (k_{ClNO_2}) and photolytic loss (j_{ClNO_2}) of $ClNO_2$. Constraining the fit to an observed median photolysis rate of $j_{ClNO_2} = 3.3 \times 10^{-4}\,s^{-1}$ (Figure S6a in Supporting Information S1) we find $k_{ClNO_2} = 2.0–5.8 \times 10^{-4}\,s^{-1}$. Aerosol surface area can vary widely across a plume transect and therefore we chose a range ($2–11 \times 10^3\,\mu m^2\,cm^{-3}$) of observed SA representative of most observations in Figure 3a (Figure S6b in Supporting Information S1) and present a sensitivity analysis to this choice in Figure S6c of Supporting Information S1. Finally, we use a median observed temperature of 296 K to find $\gamma(N_2O_5) \times \varphi(ClNO_2) = 0.3–4.7 \times 10^{-3}$.

To estimate $\varphi(ClNO_2)$ we use a laboratory-based parameterization based on observed pCl^- and calculated liquid water content, hereafter referred to as parameterized $\phi(ClNO_2)$ (Section 2.2, Text S1.4 in Supporting Information S1). Figure 3b shows parameterized $\varphi(ClNO_2)$ for all 1 Hz agriculture smoke observations, with median $\varphi(ClNO_2)$ of 0.72. When considering only observations in Figure 2a, used to determine $\gamma(N_2O_5)$, the median is 0.77. Previous field comparisons have shown that parameterized $\varphi(ClNO_2)$ is likely an upper limit to actual values (McDuffie et al., 2018a), which may, in part, be caused by the assumption that chloride is homogeneously distributed across surface area (Jeong et al., 2023; McNamara et al., 2020; Royer et al., 2021). Therefore, the derived $\gamma(N_2O_5)$ is a lower limit range of $0.2–3.6 \times 10^{-3}$.

Montane smoke plumes included several cross-wind transects downwind, which allows for $\gamma(N_2O_5)$ and $\varphi(ClNO_2)$ determination in individual plumes using a constrained 0-D chemical box model (Decker, Robinson, et al., 2021) (see Text S1.3 in Supporting Information S1). Model input values of $\gamma(N_2O_5)$ were varied between 10^{-4} and 10^{-1} to minimize the difference between the model and observations of N_2O_5. The modeled N_2O_5 is sensitive to NO_3 loss to reactions with VOCs. The model uses VOC emissions from laboratory burn emissions inventories, and these are also varied to improve the agreement between modeled and observed N_2O_5. A comparison of modeled and observed VOCs shows that the majority of the observation-model comparisons remain within the observation uncertainty. Lastly, $\varphi(ClNO_2)$ is varied between 0 and 1. Figures S7–S12 in Supporting Information S1 show complete model and observation comparisons.

Figure 3c shows a representative model to observation comparison for N_2O_5 and $ClNO_2$. In all model runs, a $\gamma(N_2O_5)$ of 10^{-4} (one order of magnitude precision, see Figure S7 in Supporting Information S1) best reproduces N_2O_5 observations. In these five cases, values of $\gamma(N_2O_5) \geq 10^{-3}$ cannot recreate the N_2O_5 observations without near or complete removal of VOCs, and values of $\gamma(N_2O_5) < 10^{-4}$ require $\varphi(ClNO_2) > 1$ to reproduce $ClNO_2$.

The box model derived $\varphi(ClNO_2)$ ranges from 0.18 to 0.80 but spans the entire 0–1 range when considering the $ClNO_2$ observational uncertainty (Figure S13 in Supporting Information S1). The average model-derived $\varphi(ClNO_2)$ is 0.45 (Figure 3d, black marker). The average of transect-center-parameterized $\varphi(ClNO_2)$ is 0.65, similar to the average of all parameterized $\varphi(ClNO_2)$ of 0.62. Parameterized $\varphi(ClNO_2)$ exceeds the box model, similar to previous field derivations (McDuffie et al., 2018a), although >90% of parameterized $\varphi(ClNO_2)$ lies within the box model derived range (Figure 3d). The derived $\varphi(ClNO_2)$ of agricultural smoke is generally greater than montane smoke, consistent with the greater pCl^- in the former. Plots of $\varphi(ClNO_2)$ against the OA:pCl^- or O:C ratio do not show clear dependences for the small number of determinations (Figure S14 in Supporting Information S1).

Values of $\gamma(N_2O_5)$ derived here are smaller than values determined in urban air ($\gamma(N_2O_5)$ $10^{-3}–10^{-1}$) (Brown & Stutz, 2012; McDuffie et al., 2018b) and comparable to or lower than a limited number of laboratory studies. A chamber study of pyrogenic aerosol for a wire grass fuel ($2.8–6 \pm 0.6 \times 10^{-3}$) and a long leaf pine needle fuel ($2.5–3.2 \pm 0.4 \times 10^{-3}$) (Goldberger et al., 2019) are similar to our agricultural fuels result. A flow-tube study of pyrogenic aerosol identified an increase of $\gamma(N_2O_5)$ for high-chloride-containing BB fuels at relative humidity (RH) >80% (Jahl et al., 2021). This is similar to the average RH (70%) for the agricultural smoke plumes here (Figure S15 in Supporting Information S1) and consistent with the observation of greater pCl^- (Figure S5 in Supporting Information S1) and larger $\gamma(N_2O_5)$ values (Figure 3) compared to montane smoke.

3.3. PyroCB Processed Smoke

The DC-8 sampled a PyroCB event produced from the Williams Flats fire on August 8 that reached 6–10 km above sea level, or 5.6 to 1.6 km below the mean tropopause height. Three visually distinct plumes were observed, and therefore we separate our analysis by plume number and transect number defined by Peterson et al. (2022).
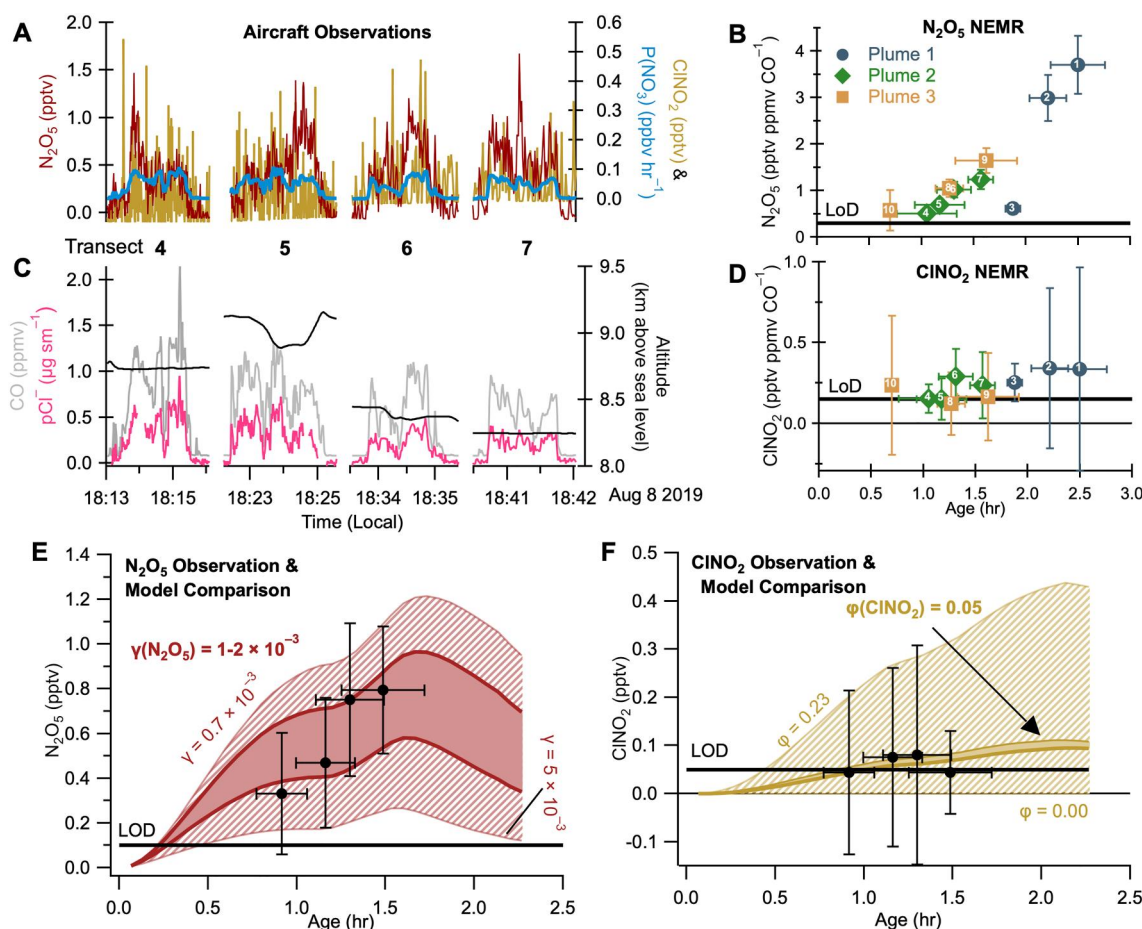
Figure 4. NASA DC-8 observations in a PyroCB on Aug 8 5.6 to 1.6 km below the mean tropopause height. Panels (a and b) show plume 2 observations only (transects 4–7). (a and c) Observations of N_2O_5 (red), $ClNO_2$ (yellow) and $P(NO_3)$ (blue), CO (gray), pCl^- (pink), and jNO_3 (black). (b and d) NEMRs of N_2O_5 and $ClNO_2$. Markers and colors indicate the plume number, and white numbers indicate the transect number. The thick black line indicates the limit of detection. E. Transect center observations of N_2O_5 (black) for plume 2 compared to the model N_2O_5 for a range (7×10^{-4}–5×10^{-3}) of $\gamma(N_2O_5)$. (f) Transect center observations of $ClNO_2$ (black) for plume 2 compared to the model-derived $ClNO_2$. Solid color is the result of a $\varphi(ClNO_2) = 0.05$ and a $\gamma(N_2O_5) = 1$–2×10^{-3} and the hashed area shows a range of possible $\varphi(ClNO_2)$.

Observed $P(NO_3)$ and N_2O_5 (Figure 4a) demonstrate the potential for heterogeneous chemistry in the PyroCB injection to the upper atmosphere. Calculated N_2O_5 NEMR increases with calculated physical plume age when separated by plume number (Figure 4b). Enhancement of pCl^- (Figure 4c) demonstrates the potential for $ClNO_2$ production. However, observations of $ClNO_2$ remained at or below the 1 Hz I^- CIMS detection limit of 0.05 pptv in Figures 4a and 4d, limiting the ability to quantify its production. Figure S16 in Supporting Information S1 shows that the $ClNO_2$ signal within all PyroCB smoke observations (average $\pm$ 1-σ of 0.03 $\pm$ 0.10 pptv) is statistically significantly greater ($p < 0.001$) than signal outside of the plume (average $\pm$ 1-σ of 0.02 $\pm$ 0.06 pptv), but the data do not allow quantification of the amount of $ClNO_2$ within the PyroCB.

Aerosol data are unavailable for plume 3, and plume 1 did not have sufficient semi-Lagrangian crosswind transects required to constrain the model. Therefore, the box model is used to derive $\gamma(N_2O_5)$ and to place an upper limit on $\varphi(ClNO_2)$ for plume 2 only. The model derived $\gamma(N_2O_5) = 0.7$–5.0×10^{-3} (Figure 4e), which is a factor of 7–50 $\times$ greater than the $\gamma(N_2O_5)$ values from plumes produced by the same fire but sampled in the lower troposphere.

The model predicts $\varphi(ClNO_2) < 0.05$ to match observations at or below the detection limit (or 0.05 at the LoD), although $\varphi(ClNO_2)$ may be up to 0.23 within the 1-σ determined $ClNO_2$ measurement uncertainty (15% + 0.05 pptv). The average parameterized $\varphi(ClNO_2)$ (0.53) is also lower than tropospheric smoke from the same fire (Figure S17 in Supporting Information S1) as a result of increased calculated liquid water fraction (LWF, Figure
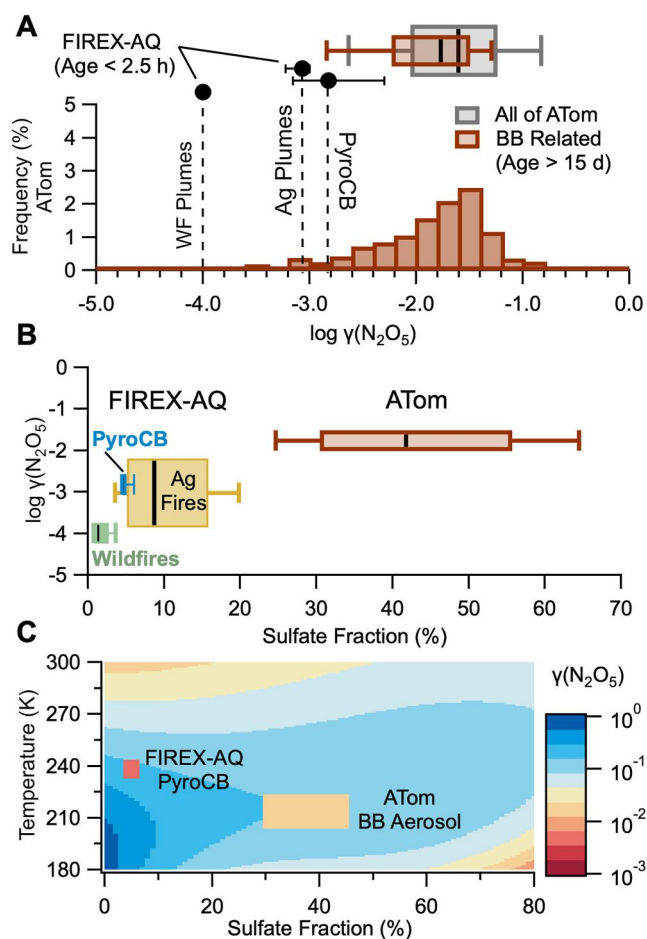
Figure 5. (a) Comparison of the model-derived $\gamma(N_2O_5)$ from FIREX-AQ and ATom. Markers show FIREX-AQ results, and the histograms show ATom BB-related $\gamma(N_2O_5)$. The box and whisker plots show the ATom BB-related (brown) and all of the ATom (gray) results from the UTLS. (b) Log γ (N_2O_5) versus aerosol sulfate fraction for FIREX-AQ and ATom. (c) γ (N_2O_5) parametrization from Burkholder et al. (2020) for aqueous sulfate particles used in stratospheric models compared to results from this work. Marker size represents the interquartile range of temperature and sulfate fraction in this work.

S18 in Supporting Information S1) in the PyroCB. The presence of sufficient pCl^- for average parameterized $\phi(ClNO_2) > 0.5$ suggests that $ClNO_2$ production may occur in PyroCB transported smoke, even if it was observed only at the detection limit in this daytime flight.

3.4. Aged UTLS Pyrogenic Aerosol

Observations from the ATom campaign provide N_2O_5 observations in the UTLS. We separate our analysis into pyrogenic-influenced and background. Air parcels with >75% of aerosol number concentration containing pyrogenic markers (see SI) are defined as pyrogenic-influenced while all others are considered background. The pyrogenic aerosol is estimated to have a physical age of >15 days. Unlike FIREX-AQ, during ATom the DC-8 did not conduct targeted sampling of plumes to constrain a semi-Lagrangian box model. Instead, a diel model built on the framework of previous model determinations of $\gamma(N_2O_5)$ in the lower troposphere (McDuffie et al., 2018b) is constrained to chemical observations (see Text S1.3 in Supporting Information S1).

The diel model predicts the median $\gamma(N_2O_5)$ from all background UTLS samples ($N = 3,483$) is 2.9×10^{-2} as shown in Figure 5a (gray box and whiskers). The pyrogenic-influenced aerosol has a median $\gamma(N_2O_5)$ of 1.7×10^{-2} (Figure 4a, brown) which is significantly different ($p < 0.001$) than the background aerosol. We also consider a smaller subset of pyrogenic influenced aerosol from ATom previously identified by Katich et al. (2023) to have originated from PyroCB influence. The resulting $\gamma(N_2O_5)$ of 2.5×10^{-2} is significantly ($p = 0.01$) less than background UTLS aerosol, and greater than our selection of pyrogeneic influenced aerosol (Figure S19 in Supporting Information S1). Overall, the model predicts that pyrogenic aerosol has a lower rate of N_2O_5 uptake than background UTLS aerosol, yet substantially greater than pyrogenic aerosol in young tropospheric plumes.

The differences in $\gamma(N_2O_5)$ across agricultural, montane, PyroCb, and UTLS data are associated with increased aerosol sulfate fraction. Figure 5b shows a positive trend in $\log(\gamma(N_2O_5))$ as a function of aerosol sulfate fraction distribution. The median sulfate fraction was 1%, 5%, 9%, and 42% in recently-emitted montane, PyroCB, agricultural and aged stratospheric BB aerosol, respectively. Laboratory studies suggest organic coatings inhibit N_2O_5 uptake, which is generally dependent on the organic layer composition and RH (Gaston et al., 2014). Conversely, increasing sulfate fraction is associated with increasing $\gamma(N_2O_5)$, potentially due to increased aerosol hygroscopicity (McDuffie et al., 2018b). Sulfate in tropospheric BB plumes arises from oxidation of pyrogenic SO_2 (Rickly et al., 2022), whereas pyrogenic-influenced aerosol in the UTLS takes up sulfate during aging.

Current stratospheric models of BB impacts on stratospheric processes (Strahan et al., 2022; Yu et al., 2021) use a γ (N_2O_5) based on purely aqueous sulfate aerosol. However, Figure 5c shows $\gamma(N_2O_5)$ values from BB influenced aerosol are a factor of 10–100 lower than pure aqueous sulfate particles (Burkholder et al., 2020). BB particles are expected to condense organics from low-volatility VOC oxidation products (Palm et al., 2020), forming organic layers that will likely reduce $\gamma(N_2O_5)$ relative to pure sulfate aerosol. Indeed, evidence of organic markers on stratospheric aerosol was found in some studies of stratospheric BB aerosol (Bernath et al., 2022; Katich et al., 2023), and BB aerosol markers are used here, by definition, to separate BB aerosol from background aerosol.

The results here indicate $\gamma(N_2O_5)$ values increase for BB particles transported from the troposphere into the UTLS, but never reach values used in stratospheric models. Some of this transport occurs through PyroCB events. Injection of the chloride-containing aerosol observed in montane smoke or repartitioning of gas phase HCl to particulate organics or reduced nitrogen (Solomon et al., 2023) may result in a non-zero $ClNO_2$ yield, thus introducing chlorine activation pathways currently not considered. Observations presented here cannot quantify

$ClNO_2$ production on BB particles transported through a PyroCB but demonstrate potential for this process. Observations of diffuse BB influenced particles in the UTLS from ATom do not have reliable $ClNO_2$ measurements, such that we are unable to assess $ClNO_2$ production on aged, dilute UTLS BB influenced particles. Concentrated BB plumes transported to the stratosphere through PyroCB events, such as the 2020 Australian fires, should have heterogeneous chemistry similar to that observed here. Recent analysis of high-altitude aircraft data suggest a ubiquitous influence of such events on stratospheric aerosol composition (Katich et al., 2023).

4. Conclusions

These results have implications for heterogeneous reactions on smoke aerosol and for smoke injection to the upper atmosphere.

Uptake coefficients for N_2O_5 determined from in situ observations are lower on BB aerosol than current model parameterizations. Figure 1 illustrates the observed trends in uptake coefficients from the lower to the upper atmosphere. The $\gamma(N_2O_5)$ on dilute smoke-impacted particles derived in this study is already lower than model parameterizations but likely represents an upper limit for more concentrated smoke such as the 2020 Australian wildfires. We therefore suggest that models of the smoke impact to the UTLS will require revised parameterizations with reduced uptake coefficients.

The recent results of Solomon et al. (2023) shows that chloride uptake by the organic phase of smoke aerosol increases heterogeneous reaction rates of halogen-containing species, thereby activating chlorine radicals that participate in ozone destruction cycles. Our results demonstrate that N_2O_5 uptake on chloride-containing smoke particles produces $ClNO_2$ in the lower atmosphere and has the potential to do so in the upper atmosphere. We suggest that $ClNO_2$ formation from N_2O_5 uptake on smoke particles injected into the stratosphere during large PyroCB events may be a component of smoke-induced halogen activation cycles that influence stratospheric ozone.

Data Availability Statement

The aircraft data used in the study are publicly available at https://www-air.larc.nasa.gov/missions/firex-aq/.

References

Ahern, A. T., Goldberger, L., Jahl, L., Thornton, J., & Sullivan, R. C. (2018). Production of N_2O_5 and $ClNO_2$ through nocturnal processing of biomass-burning aerosol. *Environmental Science & Technology*, *52*(2), 550–559. https://doi.org/10.1021/acs.est.7b04386

Akagi, S. K., Yokelson, R. J., Wiedinmyer, C., Alvarado, M. J., Reid, J. S., Karl, T., et al. (2011). Emission factors for open and domestic biomass burning for use in atmospheric models. *Atmospheric Chemistry and Physics*, *11*(9), 4039–4072. https://doi.org/10.5194/acp-11-4039-2011

Bernath, P., Boone, C., & Crouse, J. (2022). Wildfire smoke destroys stratospheric ozone. *Science*, *375*(6586), 1292–1295. https://doi.org/10.1126/science.abm5611

Bertram, T. H., Thornton, J. A., & Riedel, T. P. (2009). An experimental technique for the direct measurement of N_2O_5 reactivity on ambient particles. *Atmospheric Measurement Techniques*, *2*(2), 231–242. https://doi.org/10.5194/amt-2-231-2009

Bourgeois, I., Peischl, J., Neuman, J. A., Brown, S. S., Thompson, C. R., Aikin, K. C., et al. (2021). Large contribution of biomass burning emissions to ozone throughout the global remote troposphere. *Proceedings of the National Academy of Sciences*, *118*(52), e2109628118. https://doi.org/10.1073/pnas.2109628118

Brown, S. S., & Stutz, J. (2012). Nighttime radical observations and chemistry. *Chemical Society Reviews*, *41*(19), 6405–6447. https://doi.org/10.1039/c2cs35181a

Burkholder, J. B., Abbatt, J. P. D., Cappa, C., Dibble, T. S., Kolb, C. E., Orkin, V. L., et al. (2020). *Chemical kinetics and photochemical data for use in atmospheric studies*. JPL Publication 19-5.

Decker, Z. C. J., Robinson, M. A., Barsanti, K. C., Bourgeois, I., Coggon, M. M., DiGangi, J. P., et al. (2021). Nighttime and daytime dark oxidation chemistry in wildfire plumes: An observation and model analysis of FIREX-AQ aircraft data. *Atmospheric Chemistry and Physics*, *21*(21), 16293–16317. https://doi.org/10.5194/acp-21-16293-2021

Decker, Z. C. J., Wang, S., Bourgeois, I., Campuzano Jost, P., Coggon, M. M., DiGangi, J. P., et al. (2021). Novel analysis to quantify plume crosswind heterogeneity applied to biomass burning smoke. *Environmental Science & Technology*, *55*(23), 15646–15657. https://doi.org/10.1021/acs.est.1c03803

Dentener, F. J., & Crutzen, P. J. (1993). Reaction of N_2O_5 on tropospheric aerosols: Impact on the global distributions of NO_x, O_3, and OH. *Journal of Geophysical Research*, *98*(D4), 7149–7163. https://doi.org/10.1029/92jd02979

Gaston, C. J., Thornton, J. A., & Ng, N. L. (2014). Reactive uptake of N_2O_5 to internally mixed inorganic and organic particles: The role of organic carbon oxidation state and inferred organic phase separations. *Atmospheric Chemistry and Physics*, *14*(11), 5693–5707. https://doi.org/10.5194/acp-14-5693-2014

Goldberger, L. A., Jahl, L. G., Thornton, J. A., & Sullivan, R. C. (2019). N_2O_5 reactive uptake kinetics and chlorine activation on authentic biomass-burning aerosol. *Environmental Science: Processes & Impacts*, *21*(10), 1684–1698. https://doi.org/10.1039/C9EM00330D

Jahl, L. G., Bowers, B. B., Jahn, L. G., Thornton, J. A., & Sullivan, R. C. (2021). Response of the reaction probability of N_2O_5 with authentic biomass-burning aerosol to high relative humidity. *ACS Earth and Space Chemistry*, *5*(10), 2587–2598. https://doi.org/10.1021/acsearthspacechem.1c00227

Jeong, D., McNamara, S. M., Chen, Q., Mirrielees, J., Edebeli, J., Kulju, K. D., et al. (2023). Quantifying the Contributions of aerosol- and snow-produced $ClNO_2$ through observations and 1D modeling. *ACS Earth and Space Chemistry*, *7*(12), 2548–2561. https://doi.org/10.1021/acsearthspacechem.3c00237

Jones, M. W., Abatzoglou, J. T., Veraverbeke, S., Andela, N., Lasslop, G., Forkel, M., et al. (2022). Global and regional trends and drivers of fire under climate change. *Reviews of Geophysics*, *60*(3), e2020RG000726. https://doi.org/10.1029/2020RG000726

Katich, J. M., Apel, E. C., Bourgeois, I., Brock, C. A., Bui, T. P., Campuzano-Jost, P., et al. (2023). Pyrocumulonimbus affect average stratospheric aerosol composition. *Science*, *379*(6634), 815–820. https://doi.org/10.1126/science.add3101

Koss, A. R., Sekimoto, K., Gilman, J. B., Selimovic, V., Coggon, M. M., Zarzana, K. J., et al. (2018). Non-methane organic gas emissions from biomass burning: Identification, quantification, and emission factors from PTR-ToF during the FIREX 2016 laboratory experiment. *Atmospheric Chemistry and Physics*, *18*(5), 3299–3319. https://doi.org/10.5194/acp-18-3299-2018

Küll, V., Riese, M., Tie, X., Wiemert, T., Eidmann, G., Offermann, D., & Brasseur, G. P. (2002). NO_y partitioning and aerosol influences in the stratosphere. *Journal of Geophysical Research*, *107*(D23), 8183. https://doi.org/10.1029/2001jd001246

Liu, X., Zhang, Y., Huey, L. G., Yokelson, R. J., Wang, Y., Jimenez, J. L., et al. (2016). Agricultural fires in the southeastern U.S. during SEAC4RS: Emissions of trace gases and particles and evolution of ozone, reactive nitrogen, and organic aerosol. *Journal of Geophysical Research: Atmospheres*, *121*(12), 7383–7414. https://doi.org/10.1002/2016JD025040

May, A. A., McMeeking, G. R., Lee, T., Taylor, J. W., Craven, J. S., Burling, I., et al. (2014). Aerosol emissions from prescribed fires in the United States: A synthesis of laboratory and aircraft measurements. *Journal of Geophysical Research: Atmospheres*, *119*(20), 11826–11849. https://doi.org/10.1002/2014JD021848

McDuffie, E. E., Fibiger, D. L., Dubé, W. P., Lopez Hilfiker, F., Lee, B. H., Jaeglé, L., et al. (2018a). $ClNO_2$ yields from aircraft measurements during the 2015 WINTER campaign and critical evaluation of the current parameterization. *Journal of Geophysical Research: Atmospheres*, *123*(22), 12994–13015. https://doi.org/10.1029/2018JD029358

McDuffie, E. E., Fibiger, D. L., Dubé, W. P., Lopez-Hilfiker, F., Lee, B. H., Thornton, J. A., et al. (2018b). Heterogeneous N_2O_5 uptake during winter: Aircraft measurements during the 2015 WINTER campaign and critical evaluation of current parameterizations. *Journal of Geophysical Research: Atmospheres*, *123*(8), 4345–4372. https://doi.org/10.1002/2018JD028336

McNamara, S. M., Kolesar, K. R., Wang, S., Kirpes, R. M., May, N. W., Gunsch, M. J., et al. (2020). Observation of road salt aerosol driving inland wintertime atmospheric chlorine chemistry. *ACS Central Science*, *6*(5), 684–694. https://doi.org/10.1021/acscentsci.9b00994

Palm, B. B., Peng, Q., Fredrickson, C. D., Lee, B. H., Garofalo, L. A., Pothier, M. A., et al. (2020). Quantification of organic aerosol and brown carbon evolution in fresh wildfire plumes. *Proceedings of the National Academy of Sciences*, *117*(47), 29469–29477. https://doi.org/10.1073/pnas.2012218117

Peterson, D. A., Fromm, M. D., McRae, R. H. D., Campbell, J. R., Hyer, E. J., Taha, G., et al. (2021). Australia's Black Summer pyrocumulonimbus super outbreak reveals potential for increasingly extreme stratospheric smoke events. *npj Climate and Atmospheric Science*, *4*(1), 38. https://doi.org/10.1038/s41612-021-00192-9

Peterson, D. A., Thapa, L. H., Saide, P. E., Soja, A. J., Gargulinski, E. M., Hyer, E. J., et al. (2022). Measurements from inside a Thunderstorm driven by wildfire: The 2019 FIREX-AQ field experiment. *Bulletin of the American Meteorological Society*. https://doi.org/10.1175/BAMS-D-21-0049.1

Ravishankara, A. R. (1997). Heterogeneous and multiphase chemistry in the troposphere. *Science*, *276*(5315), 1058–1065. https://doi.org/10.1126/science.276.5315.1058

Rickly, P. S., Guo, H., Campuzano-Jost, P., Jimenez, J. L., Wolfe, G. M., Bennett, R., et al. (2022). Emission factors and evolution of SO_2 measured from biomass burning in wildfires and agricultural fires. *Atmospheric Chemistry and Physics*, *22*(23), 15603–15620. https://doi.org/10.5194/acp-22-15603-2022

Roberts, J. M., Osthoff, H. D., Brown, S. S., Ravishankara, A. R., Coffman, D., Quinn, P., & Bates, T. (2009). Laboratory studies of products of N_2O_5 uptake on Cl-containing substrates. *Geophysical Research Letters*, *36*(20), L20808. https://doi.org/10.1029/2009GL040448

Royer, H. M., Mitroo, D., Hayes, S. M., Haas, S. M., Pratt, K. A., Blackwelder, P. L., et al. (2021). The role of hydrates, competing chemical constituents, and surface composition on $ClNO_2$ formation. *Environmental Science & Technology*, *55*(5), 2869–2877. https://doi.org/10.1021/acs.est.0c06067

Solomon, S. (1999). Stratospheric ozone depletion: A review of concepts and history. *Reviews of Geophysics*, *37*(3), 275–316. https://doi.org/10.1029/1999rg900008

Solomon, S., Dube, K., Stone, K., Yu, P., Kinnison, D., Toon Owen, B., et al. (2022). On the stratospheric chemistry of midlatitude wildfire smoke. *Proceedings of the National Academy of Sciences*, *119*(10), e2117325119. https://doi.org/10.1073/pnas.2117325119

Solomon, S., Stone, K., Yu, P., Murphy, D. M., Kinnison, D., Ravishankara, A. R., & Wang, P. (2023). Chlorine activation and enhanced ozone depletion induced by wildfire aerosol. *Nature*, *615*(7951), 259–264. https://doi.org/10.1038/s41586-022-05683-0

Strahan, S. E., Smale, D., Solomon, S., Taha, G., Damon, M. R., Steenrod, S. D., et al. (2022). Unexpected repartitioning of stratospheric inorganic chlorine after the 2020 Australian wildfires. *Geophysical Research Letters*, *49*(14), e2022GL098290. https://doi.org/10.1029/2022GL098290

Thompson, C. R., Wofsy, S. C., Prather, M. J., Newman, P. A., Hanisco, T. F., Ryerson, T. B., et al. (2022). The NASA Atmospheric Tomography (ATom) Mission: Imaging the chemistry of the global atmosphere. *Bulletin of the American Meteorological Society*, *103*(3), E761–E790. https://doi.org/10.1175/BAMS-D-20-0315.1

Wang, X., Jacob, D. J., Eastham, S. D., Sulprizio, M. P., Zhu, L., Chen, Q., et al. (2019). The role of chlorine in global tropospheric chemistry. *Atmospheric Chemistry and Physics*, *19*(6), 3981–4003. https://doi.org/10.5194/acp-19-3981-2019

Warneke, C., Schwarz, J. P., Dibb, J., Kalashnikova, O., Frost, G., Al-Saad, J., et al. (2023). Fire Influence on Regional to Global Environments and Air Quality (FIREX-AQ). *Journal of Geophysical Research: Atmospheres*, *128*(2), e2022JD037758. https://doi.org/10.1029/2022JD037758

Wofsy, S. C., Afshar, S., Allen, H. M., Apel, E. C., Asher, E. C., Barletta, B., et al. (2018). In ORNL DAAC (Ed.), *ATom: Merged Atmospheric Chemistry, Trace Gases, and Aerosols*.

Xu, L., Crounse John, D., Vasquez Krystal, T., Allen, H., Wennberg Paul, O., Bourgeois, I., et al. (2021). Ozone chemistry in western U.S. wildfire plumes. *Science Advances*, *7*(50), eabl3648. https://doi.org/10.1126/sciadv.abl3648

Yu, P., Davis, S. M., Toon, O. B., Portmann, R. W., Bardeen, C. G., Barnes, J. E., et al. (2021). Persistent stratospheric warming due to 2019–2020 Australian wildfire smoke. *Geophysical Research Letters*, *48*(7), e2021GL092609. https://doi.org/10.1029/2021GL092609

Zambri, B., Solomon, S., Kinnison, D. E., Mills, M. J., Schmidt, A., Neely, III, R. R., et al. (2019). Modeled and observed volcanic aerosol control on stratospheric NO_y and Cl_y. *Journal of Geophysical Research: Atmospheres*, *124*(17–18), 10283–10303. https://doi.org/10.1029/2019JD031111